K was found. Cooling the crystals resulted in a contraction of the lattice parameter by ~1%, a broadening of the reflections by a factor of nearly 2, and an increase in the rate of crystal decomposition. Due to the higher mosaic spread of the crystals, the limit of resolution of the data was substantially lower than at ambient temperature. An electron-density difference map calculated after refinement of the non-H atom parameters was indistinguishable from the maps calculated using the room temperature data. Only model e was refined. The Co^{II}–N bond length was 2.164 (4) Å.

Discussion

The structure consists of Co atoms at the positions of a face-centered cubic lattice, Cl^- anions at all combinations of $\pm^1/_4$, $\pm^1/_4$, $\pm^1/_4$, N atoms lying along the axes, and H atoms disordered on circles perpendicular to and centered on the axes (Figure 2). The NH_3 ligands make contacts with the Cl^- anions at distances which are consistent with weak hydrogen bonds. There are four symmetry-related Cl^- anions arranged around each NH_3 ligand, but in any orientation of the ligand only one H atom can be in the optimum position for forming a N–H···Cl bond. It is probable that the observed maxima in the H atom electron density at 90° intervals are a consequence of the H-bonding interactions. There are no significant nonbonded contacts within the lattice, the shortest $Cl^-\cdots Cl^-$ distance being 5.07 Å.

The length of the Co^{II}–N bond in $[Co(NH_3)_6]Cl_2$ found in the present study, 2.170 (2) Å, is the most precise value reported to date. Similar bond-lengths occur in $[Co^{II}(tacn)_2]I_2$ (2.155 (15) Å),[17] $[Co^{II}$(sepulchrate)$](S_2O_6)$ (average 2.164 (12) Å),[17] $[Co(NH_3)_6](PF_6)_2$ (2.183 (2) Å),[19] and $[Co(NH_3)_6](BF_4)_2$ (2.186 (10) Å).[19] The significantly lower value in the complex of the macrocyclic ligand tacn[20] is due to steric constraints; both it and the unstrained value in the sepulchrate[20] complex are well reproduced by molecular-mechanics calculations.[21] The structures of $[Co(NH_3)_6](PF_6)_2$ and $[Co(NH_3)_6](BF_4)_2$ were refined in the same space group as $[Co(NH_3)_6]Cl_2$, $Fm\bar{3}m$.[19] These salts differ from $[Co(NH_3)_6]Cl_2$ by having anions that do not form strong hydrogen bonds with NH_3. The infrared spectra are consistent with hydrogen bonding in $[Co(NH_3)_6]Cl_2$ but not in $[Co(NH_3)_6](PF_6)_2$ and $[Co(NH_3)_6](BF_4)_2$.[19]

In the time that has elapsed since the 1969 comparison between the Co–N bond lengths in $[Co(NH_3)_6]Cl_2$ and $[Co(NH_3)_6]I_3$,[9] the structures of a number of other $[Co(NH_3)_6]^{3+}$ salts have been reported. In most cases, the achievement of high precision was hampered by large unit cells, disorder, and/or high thermal motion. For example, 11 Co^{III}–N bond lengths ranging from 1.955 (9) to 1.983 (11) Å (with a mean of 1.966 Å) were derived from the structure of $[Co(NH_3)_6]Cl_3$ which crystallizes with an asymmetric unit of four formula units.[22] The most precise published value for the Co^{III}–N bond length in a $[Co(NH_3)_6]^{3+}$ salt is 1.965 (1) Å in $[Co(NH_3)_6][FeCl_6]$.[23] We conclude that the current best estimate of the difference between the Co–N bond lengths in $[Co^{II}(NH_3)_6]^{2+}$ and $[Co^{III}(NH_3)_6]^{3+}$ is 0.205 (3) Å.

Acknowledgment. This work was supported by a grant from the Australian Research Grants Scheme (A2860032P).

Supplementary Material Available: Tables S2 and S3, listing additional crystal data specifications and positional and thermal parameters at 128 K (2 pages); Table S1, listing observed and calculated structure factors (1 page). Ordering information is given on any current masthead page.

(17) Küppers, H.-J.; Neves, A.; Pomp, C.; Ventur, D.; Wieghardt, K.; Nuber, B.; Weiss, J. *Inorg. Chem.* **1986**, *25*, 2400–2408.
(18) Creaser, I. I.; Geue, R. J.; Harrowfield, J. MacB.; Herlt, A. J.; Sargeson, A. M.; Snow, M. R.; Springborg, J. *J. Am. Chem. Soc.* **1982**, *104*, 6016–6025.
(19) Kummer, S.; Babel, D. *Z. Naturforsch.* **1984**, *39B*, 1118–1122.
(20) Key: tacn, 1,4,7-triazacyclononane; sepulchrate, 1,3,6,8,10,13,16,19-octaazabicyclo[6.6.6]eicosane.
(21) Hambley, T. W. *Inorg. Chem.* **1988**, *27*, 2456–2501.
(22) Kruger, G. J.; Reynhardt, E. C. *Acta Crystallogr.* **1978**, *B34*, 915–917.
(23) Beattie, J. K.; Moore, C. J. *Inorg. Chem.* **1982**, *21*, 1292–1295.

Contribution from the Department of Chemistry, York University, North York, Ontario, Canada M3J 1P3

Bis(dioxolene)bis(pyridine)ruthenium Redox Series

Pamela R. Auburn,[1a] Elaine S. Dodsworth, Masa-aki Haga,[1b] Wei Liu,[1c] W. Andrew Nevin,[1d] and A. B. P. Lever*

Received December 28, 1990

A series of ruthenium complexes containing noninnocent 1,2-dioxolene ligands (dioxolene refers to any of the series catechol–semiquinone–quinone) have been prepared. These have the formula *t*-$[Ru(RPy)_2(dioxolene)_2]^n$, where the RPy ligands are a series of substituted pyridines and $n = -1, 0, +1$. Their electrochemical and spectroscopic (NMR, ESR, IR, PES, electronic) properties are reported and discussed in terms of their electronic structures, described by using simple qualitative molecular orbital models. Their electronic structures are subtly different from those of the related *c*-$[Ru(bpy)(dioxolene)_2]^n$ species reported previously (bpy = 2,2′-bipyridine). The neutral ($n = 0$) complexes have a fully delocalized, mixed-valence $Ru^{III}(RPy)_2$(catechol)(semiquinone) electronic structure. The oxidized ($n = +1$) and reduced ($n = -1$) species are also Ru^{III} species. The electronic absorption data show a variety of different charge-transfer bands whose assignments are based upon energy variations with change of pyridine and/or dioxolene substituent and upon the net oxidation state.

Introduction

1,2-Dioxolenes, members of the catechol–semiquinone–quinone redox chain, have orbitals that are close in energy to the transition-metal d orbitals. The charge distribution in dioxolene coordination complexes depends upon the relative energies and overlap of these metal and dioxolene ligand orbitals.[2,3] In general, the energies are sufficiently disparate that the metal and dioxolene levels remain discrete within the electronic structures of these complexes. This is in sharp contrast to the closely related dithiolene ligands, which form complexes characterized by extensive

Chart I

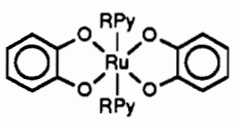

(1) Current addresses: (a) Chevron Chemical Co., Kingwood, TX. (b) Department of Chemistry, Mie University, Japan. (c) Department of Chemistry, Yangzhou Teacher's College, Jiangsu, People's Republic of China. (d) Central Research Laboratories, Kanegafuchi Chemical Industry Co. Ltd., Kobe 652, Japan.
(2) Pierpont, C. G.; Buchanan, R. M. *Coord. Chem. Rev.* **1981**, *38*, 45.
(3) Kaim, W. *Coord. Chem. Rev.* **1987**, *76*, 187.

0020-1669/91/1330-3502$02.50/0

electron delocalization.[4,5] We recently reported studies of redox series based upon the $Ru(bpy)_2$(dioxolene) and Ru(bpy)(dioxolene)$_2$ species (bpy = 2,2'-bipyridine) and provided evidence for the first highly delocalized dioxolene complexes.[6-9] Similar behavior has also been demonstrated for related osmium complexes[10] and Ru(dioxolene)$_3$.[11]

We now report a series of analogous *t*-Ru(RPy)$_2$(R'Diox)$_2$ complexes (Chart I). These species are more amenable to synthetic variation and thus allow a systematic study of the factors influencing the electronic structures of these materials. The bis(pyridine) complexes are initially isolated in the trans geometric configuration, but can be isomerized readily to cis isomers. The kinetic and mechanistic aspects of this isomerization will be reported separately.[12]

In the discussion that follows, the abbreviation R'Diox is used for a dioxolene of unspecified oxidation state, while the abbreviations q, sq, and cat are used to specify the quinone, semiquinone, and catechol oxidation states. Thus for instance, DTBDiox is a general term for DTBCat, DTBSq, or DTBQ. As in the previous study,[9] the symbol S is used for the initially derived starting material, and O1, O2, R1, and R2 are used for the first and second oxidized and first and second reduced species, respectively. The symbols *c* and *t* designate cis and trans isomers.

Experimental Section

Methods. Electronic spectra in the visible and near-infrared (near-IR) were recorded with a Perkin-Elmer microprocessor Model 340 spectrometer. Fourier transform infrared (FTIR) data were obtained by using a Nicolet SX20 spectrometer. Samples were prepared as KBr pellets or as Nujol or hexachlorobutadiene (HCBD) mulls. NMR spectra were obtained on a Bruker AM 300 FT NMR spectrometer. Photoelectron spectra (PES) were collected by the Surface Science Centre at the University of Western Ontario, London, Ontario, Canada. Magnetic data were obtained, courtesy of Professor L.K. Thompson (Memorial University of Newfoundland), using a Faraday magnetometer (see ref 13 for details). Electron spin resonance (ESR) spectra were obtained with a Varian E4 spectrometer and were calibrated against diphenylpicrylhydrazide (DPPH).

Electrochemical data were collected with a Princeton Applied Research (PARC) Model 173 potentiostat or a PARC Model 174 polarographic analyzer, coupled to a PARC Model 175 universal programmer. Cyclic and differential-pulse voltammetries were carried out by using platinum wires as working and counter electrodes, and a AgCl/Ag quasi-reference electrode with ferrocene (Fc) as an internal standard. The Fc^+/Fc couple was assumed to lie at +0.425 V vs SCE;[14] this appears to be a more realistic value than those cited in our earlier work.[6,9] Spectroelectrochemical experiments utilized a modified 1-cm glass cuvette equipped with a AgCl/Ag reference electrode, a Nichrome-wire counter electrode, and a platinum-gauze working electrode. The reference and counter electrodes were each separated from the bulk solution by a sintered glass frit.

Materials. Tetrabutylammonium perchlorate (TBAP, Kodak) and tetrabutylammonium hexafluorophosphate (TBAH, Aldrich) were recrystallized from absolute ethanol and dried in a vacuum oven at 50 °C for 2 days. *o*-Dichlorobenzene (DCB, Aldrich Gold Label) was used as supplied. 1,2-Dichloroethane (DCE, BDH Omnisolve) was dried and distilled from P_2O_5. Dichloromethane (DCM, BDH Analytical) was dried over CaH_2 and diethyl ether over $LiAlH_4$, and both were distilled under nitrogen prior to use. 3,5-Di-*tert*-butylcatechol ($DTBCatH_2$, Aldrich) and 4-*tert*-butylcatechol ($TBCatH_2$, Aldrich) were recrystallized from ethanol. Catechol ($CatH_2$), 4-methylcatechol ($MeCatH_2$), and 4-chlorocatechol ($ClCatH_2$) were obtained from Tokyo Kasei and used as supplied. Pyridine and pyridine derivatives (Aldrich) were distilled or recrystallized prior to use. 4-Chloropyridine hydrochloride (Aldrich) was used as supplied. Cobaltocene (Cp_2Co, Strem) was sublimed prior to use. Silver salts, $AgClO_4$, $AgSO_3CF_3$, and $AgPF_6$ (Aldrich), were used as supplied. $[Ru_2(OAc)_4Cl]_n$ was prepared according to a published procedure.[15]

Preparation of Complexes. ***t*-Ru(Py)$_2$(DTBDiox)$_2$.** DTBDiox is derived from 3,5-di-*tert*-butylcatechol. To a boiling mixture of $[Ru_2OAc_4Cl]_n$ (0.4 g, 0.84 mmol) and $DTBCatH_2$ (0.753 g, 3.39 mmol) in methanol (50 mL) under nitrogen was added a solution of NaOH (0.27 g, 6.77 mmol) in methanol (15 mL). The solids dissolved to give a deep purple solution to which, after 1 h, pyridine (1 mL) was added. After an additional 5 h of refluxing, the resultant orange-brown solution was exposed to the atmosphere and filtered. During this procedure, the solution became blue-green in color. The filtrate was allowed to cool and then stand at ambient temperature for 12 h. Black-green needles of the product were isolated by filtration, washed with methanol, and air-dried.

***t*-Ru(RPy)$_2$(R'Diox)$_2$.** RPy is 3- or 4-acetylpyridine (3-AcPy, 4-AcPy), 3- or 4-chloropyridine (3-ClPy, 4-ClPy), 3- or 4-phenylpyridine (3-PhPy, 4-PhPy), 4-vinylpyridine (4-VPy), 4-picoline (4-MePy), 3- or 4-ethylpyridine (3-EtPy, 4-EtPy), or 4-butylpyridine (4-BuPy), and R'Diox is derived from 3,5-di-*tert*-butylcatechol, 4-*tert*-butylcatechol, 4-methylcatechol, catechol or 4-chlorocatechol. These complexes were prepared, with the appropriate ligand partners, by following the procedure above. When the 4-ClPy ligand was required, it was generated in situ from the hydrochloride by use of an additional stoichiometric amount of base in the above procedure. The solubilities of the reaction products varied. Filtrates containing 3-AcPy or 4-AcPy complexes required concentration before the product would crystallize, whereas complexes containing the 4-PhPy or 3-PhPy ligands precipitated from the hot reaction mixtures before filtration. Products so isolated, washed with methanol, and air-dried were found to be pure. Yields were between 10 and 40%. Analytical data and yields are given as supplementary material (Table SI).

***t*-[Ru(3-ClPy)$_2$(DTBDiox)$_2$]ClO$_4$.** To a stirred solution of *t*-Ru(3-ClPy)$_2$(DTBDiox)$_2$ (46.2 mg, 0.06 mmol) in dry dichloromethane (10 mL), under nitrogen, was added dropwise a solution of $AgClO_4$ (12.5 mg, 0.06 mmol) in acetonitrile (1 mL). During the addition, the solution changed in color from yellow-green to blue. The mixture was stirred at ambient temperature for 3 h. The precipitated metallic silver was removed by filtration through a short plug of Celite. The filtrate was concentrated under reduced pressure and diethyl ether was added to initiate crystallization. The mixture was stored at −5 °C for 72 h. Dark blue crystals of the product (41.5 mg, 78%) were isolated by filtration, washed with diethyl ether, and air-dried.

***t*-[Ru(RPy)$_2$(R'Diox)$_2$]X (X$^-$ = ClO_4^-, PF_6^-, $SO_3CF_3^-$).** These compounds were prepared by analogous procedures using the appropriate ruthenium complex and silver salt. The solubilities of the reaction products varied slightly, and occasionally a mixture of diethyl ether and hexanes, or hexanes alone, was required to initiate crystallization. The yields for these reactions varied between 75 and 95%. Analytical data are given in Table SII (supplementary material). For spectroscopic purposes, some of these O1 materials were generated in situ by the addition of the appropriate silver salt to a solution of the ruthenium S complex. Solutions prepared in this manner were filtered prior to spectroscopic measurements.

[Cp$_2$Co][Ru(3-ClPy)$_2$(DTBDiox)$_2$]. This reaction was carried out in a Vacuum Atmospheres drybox. To cobaltocene (40.5 mg, 0.27 mmol) was added a solution of Ru(3-ClPy)$_2$(DTBDiox)$_2$ (150 mg, 0.19 mmol) in dichloromethane (10 mL). A dark green solid precipitated from the resultant mauve solution. The mixture was stirred for about 30 min to digest the precipitate, and the solid was then allowed to settle (2 h). Dark green crystals (122 mg, 67%) were isolated by filtration, washed sequentially with dichloromethane, diethyl ether, and hexanes, and dried in vacuo. Anal. Calcd for $RuCoC_{48}H_{58}Cl_2N_2O_4$: C, 60.19; H, 6.10; N, 2.92. Found: C, 59.67; H, 6.02; N, 2.90.

For spectroscopic measurements this and other R1 species were prepared in situ by reduction of the appropriate ruthenium S complex with cobaltocene. For ESR experiments the best results were obtained by using a slight deficiency of cobaltocene to ensure that the cobaltocene

(4) McCleverty, J. A. *Prog. Inorg. Chem.* **1968**, *10*, 49.
(5) Schrauzer, G. N. *Acc. Chem. Res.* **1969**, *2*, 72.
(6) Haga, M.; Dodsworth, E. S.; Lever, A. B. P. *Inorg. Chem.* **1986**, *25*, 447.
(7) Haga, M.; Dodsworth, E. S.; Lever, A. B. P.; Boone, S. R.; Pierpont, C. G. *J. Am. Chem. Soc.* **1986**, *108*, 7413.
(8) Stufkens, D. J.; Snoeck, Th. L.; Lever, A. B. P. *Inorg. Chem.* **1988**, *27*, 953.
(9) Lever, A. B. P.; Auburn, P. R.; Dodsworth, E. S.; Haga, M.; Liu, W.; Melnik, M.; Nevin, W. A. *J. Am. Chem. Soc.* **1988**, *110*, 8076.
(10) Haga, M.; Isobe, K.; Boone, S. R.; Pierpont, C. G. *Inorg. Chem.* **1990**, *29*, 3795.
(11) Bhattacharya, S.; Boone, S. R.; Fox, G. A.; Pierpont, C. G. *J. Am. Chem. Soc.* **1990**, *112*, 1088.
(12) Tse, Y.-H.; Auburn, P. R.; Lever, A. B. P. To be submitted for publication.
(13) Wen, T.; Thompson, L. K.; Lee, F. L.; Gabe, E. J. *Inorg. Chem.* **1988**, *27*, 4190.
(14) Gennett, T.; Milner, D. F.; Weaver, M. J. *J. Phys. Chem.* **1985**, *89*, 2787.
(15) Mitchell, R. W.; Spencer, A.; Wilkinson, G. *J. Chem. Soc., Dalton Trans.* **1973**, 846.

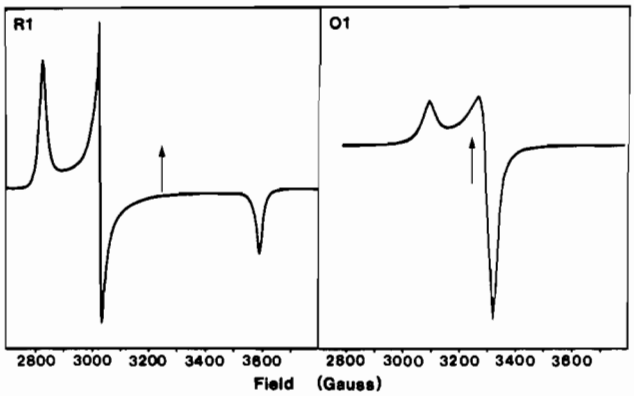

Figure 1. ESR spectra of (left) R1 $[Cp_2Co][Ru(3\text{-}ClPy)_2(DTBDiox)_2]$, and (right) $[Ru(4\text{-}MePy)_2(DTBDiox)_2]ClO_4$, both in the solid state at 77 K. The arrows denote the positions of the DPPH signals.

signal did not interfere with the spectrum of the reduced ruthenium complex.

Some representative colors of solutions are as follows:

	R1	S	O1
$Ru(Py)_2(DTBDiox)_2$	yellow-brown	yellow-green	deep blue
$Ru(4\text{-}BuPy)_2(ClDiox)_2$	yellow-green	violet	blue-green

Results

The starting materials, S, and the one-electron oxidized species, O1, are air-stable, crystalline solids. The crystal structures of one S and one O1 species have been reported,[7,16,17] and are discussed below. Both possess a trans-C_{2h} structure in which the two pyridine planes are parallel and bisect the plane containing the dioxolene ligands. One example of the air-sensitive one-electron reduction product, R1, was also isolated in the solid state.

Nuclear Magnetic Resonance Spectra. ^1H NMR data for the even electron starting materials, S, are given in Table I. The ^1H NMR spectra are sharp and are temperature-invariant between −60 and +60 °C. The DTBDiox complexes give ^1H and ^{13}C NMR spectra consistent with the presence of only one trans isomer in solution. Solutions of $Ru(3\text{-}ClPy)_2(TBDiox)_2$, $Ru(4\text{-}PhPy)_2(TBDiox)_2$, and $Ru(4\text{-}VPy)_2(TBDiox)_2$ all show a single *tert*-butyl resonance in the aliphatic spectral region of their ^1H NMR spectra but show two doublets of doublets around 6 ppm due to the protons in the 5-positions of the 4-*tert*-butyldioxolene ligands. Selective decoupling of each individual doublet of doublets in the spectrum of $Ru(4\text{-}VPy)_2(TBDiox)_2$ resulted in the collapse of the doublets due to protons in the 3- and 6-positions of the corresponding isomer.

Magnetism and Electron Spin Resonance. The starting materials (S) are diamagnetic on the basis of their NMR spectra and ESR silence at room temperature or 77 K (solution and solid state). Magnetic measurements on an O1 complex, $[Ru(4\text{-}MePy)_2(DTBDiox)_2]ClO_4$, show one unpaired electron. This complex shows Curie–Weiss behavior (equation of line $\chi_M(cor) = 0.376/(T + 7.81)$; $R = 0.998$) and has magnetic moments of 1.74 and 1.54 μ_B at 295 and 5.65 K respectively.

The ESR spectra of the $S = {}^1/_2$ O1 and R1 species, at room temperature in solution or the solid state, are either broad with g values close to 2 or are undetectable. Signals are observed for all of these species at low temperatures, 77–115 K (Tables II and III; Figure 1). The O1 signals, in frozen DCE solutions, are broad and centered near the free-radical value of $g = 2$. Frozen DCE solutions of the R1 species exhibit highly anisotropic signals with two or three distinct g values.

Electrochemistry. The electrochemical behavior of these species is very similar to that of the $Ru(bpy)(R'Diox)_2$ complexes. Redox chains containing five members may be characterized by cyclic voltammetry of the starting materials (Table IV). The bulk solution rest potentials lie between couples II and III (Figure 2).

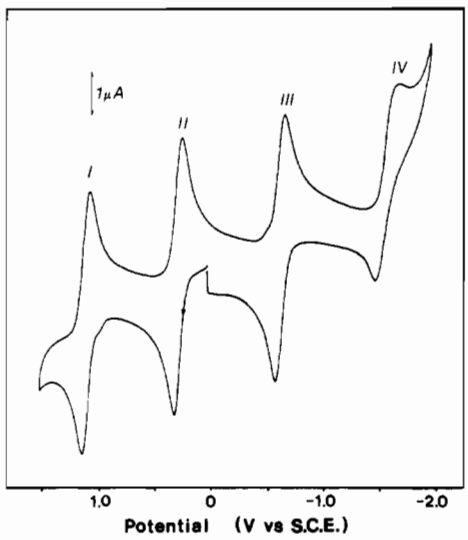

Figure 2. Cyclic voltammogram of 8.5×10^{-4} M $Ru(4\text{-}ClPy)_2(DTBDiox)_2$ in DCE solution containing 0.2 M TBAH. Scan rate: 100 mV s^{-1}.

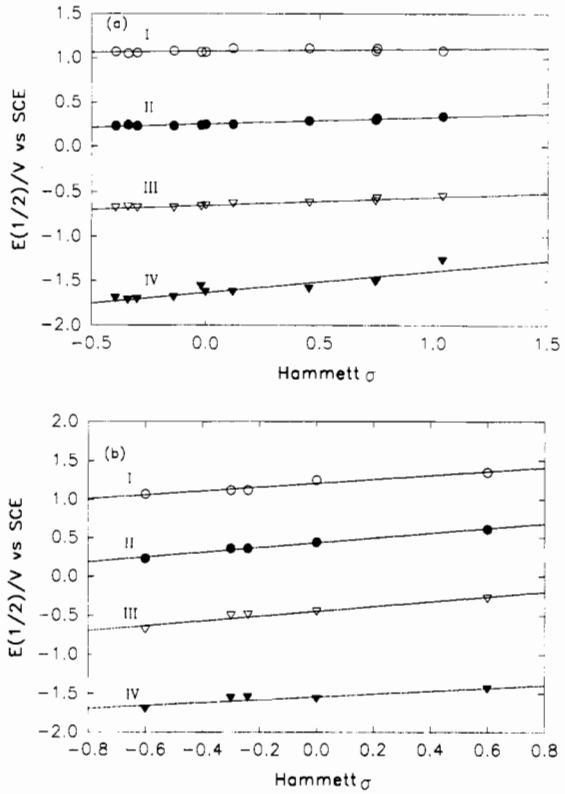

Figure 3. Variation of the redox potentials of (a) $Ru(RPy)_2(DTBDiox)_2$ complexes with the Hammett σ parameters for the pyridine substituents (slopes: I, 0.02; II, 0.08; III, 0.09; IV, 0.24) and (b) $Ru(4\text{-}BuPy)_2(R'Diox)_2$ complexes with the Hammett σ parameters for the dioxolene substituents (slopes: I, 0.25; II, 0.31; III, 0.31; IV, 0.19). The Hammett parameters are multiplied by the number of substituents in the complex. For the 4-R'Diox complexes the para and meta parameters are averaged to account for the substituent effect at both oxygens. For DTBDiox the average of the para and meta σ values is doubled to account for both *tert*-butyl groups, assuming the substituent effects for the ortho and para positions are equal.

The variations of the redox potentials as functions of the pyridine and dioxolene substituents, using the Hammett σ parameters,[18] are shown in Figure 3.

Couples I–III are reversible ($i_p \propto v^{1/2}$, $i_c/i_a = 1$) for all species, with peak to peak separations of 65–85 mV at 100 mV s^{-1} in DCE.

(16) Boone, S. R.; Pierpont, C. G. *Inorg. Chem.* **1987**, *26*, 1769.
(17) Boone, S. R.; Pierpont, C. G. *Polyhedron* **1990**, *9*, 2267.
(18) Hammett, L. P. *Physical Organic Chemistry, Reaction Rates, Equilibria and Mechanisms*, 2nd ed.; McGraw Hill: New York, 1970.

Table I. ^{1}H NMR Spectra of *t*-Ru(RPy)$_2$(R′Diox)$_2$, S, Complexes[a]

complex	chem shift, δ
Ru(3-AcPy)$_2$(DTBDiox)$_2$	8.03 (d, *J* = 1.6 Hz, 2 H), 7.83 (m, 2 H), 7.71 (d, 2.1 Hz, 2 H), 7.68 (dd, *J* = 5.6, 1.4 Hz, 2 H), 7.00 (dd, *J* = 7.9, 5.7 Hz, 2 H), 6.20 (d, *J* = 2.1 Hz, 2 H), 2.34 (s, 6 H), 1.65 (s, 18 H), 1.37 (s, 18 H)
Ru(4-AcPy)$_2$(DTBDiox)$_2$	7.84 (d, *J* = 6.9 Hz, 2 H), 7.62 (d, *J* = 2.1 Hz, 4 H), 7.28 (dd, *J* = 6.8, 1.5 Hz, 4 H), 6.27 (br s, 2 H), 2.40 (s, 6 H), 1.64 (s, 18 H), 1.36 (s, 18 H)
Ru(3-ClPy)$_2$(DTBDiox)$_2$	7.74 (d, *J* = 2.2 Hz, 2 H), 7.63 (d, *J* = 2.0 Hz, 2 H), 7.60 (dd, *J* = 5.4, 1.1 Hz, 2 H), 7.23 (m, 2 H), 6.87 (dd, *J* = 8.2, 5.7 Hz, 2 H), 6.17 (br s, 2 H), 1.62 (s, 18 H), 1.35 (s, 18 H)
Ru(4-ClPy)$_2$(DTBDiox)$_2$	7.66 (d, *J* = 2.1 Hz, 2 H), 7.51 (dd, *J* = 5.4, 1.3 Hz, 4 H), 6.84 (dd, *J* = 5.4, 1.3 Hz, 4 H), 6.13 (d, *J* = 1.9 Hz, 2 H), 1.64 (s, 18 H), 1.38 (s, 18 H)
Ru(3-PhPy)$_2$(DTBDiox)$_2$	7.79 (d, *J* = 2.1 Hz, 2 H), 7.67 (d, *J* = 1.9 Hz, 2 H), 7.40 (m, 2 H), 7.31 (m, 2 H), 7.26 (m, 10 H), 6.87 (m, 2 H), 6.09 (d, *J* = 2.1 Hz, 2 H), 1.63 (s, 18 H), 1.40 (s, 18 H)
Ru(Py)$_2$(DTBDiox)$_2$	7.64 (s, 2 H), 7.51 (d, *J* = 5.1 Hz, 4 H), 7.22 (t, *J* = 7.5 Hz, 2 H), 6.79 (dd, *J* = 7.5, 5.1 Hz, 4 H), 5.92 (br s, 2 H), 1.61 (s, 18 H), 1.40 (s, 18 H)
Ru(4-PhPy)$_2$(DTBDiox)$_2$	7.70 (d, *J* = 2.2, 2 H), 7.50 (d, *J* = 6.9 Hz, 4 H), 7.35 (br s, 10 H), 7.02 (d, 6.6 Hz, 4 H), 6.02 (d, *J* = 2.2 Hz, 2 H), 1.68 (s, 18 H), 1.41 (s, 18 H)
Ru(4-VPy)$_2$(DTBDiox)$_2$	7.75 (br s, 2 H), 7.40 (d, *J* = 6.1 Hz, 4 H), 6.77 (d, *J* = 6.1 Hz, 4 H), 6.36 (dd, *J* = 17.5, 10.8 Hz, 2 H), 5.96 (br s, 2 H), 5.70 (d, *J* = 17.5, 2 H), 5.34 (d, *J* = 10.8 Hz, 2 H), 1.66 (s, 18 H), 1.48 (s, 18 H)
Ru(4-MePy)$_2$(DTBDiox)$_2$	7.78 (d, *J* = 2.1 Hz, 2 H), 7.20 (d, *J* = 6.6 Hz, 4 H), 6.59 (d, *J* = 5.9 Hz, 4 H), 5.95 (d, *J* = 1.9 Hz, 2 H), 2.17 (s, 6 H), 1.65 (s, 18 H), 1.42 (s, 18 H)
Ru(3-EtPy)$_2$(DTBDiox)$_2$	7.77 (br s, 2 H), 7.27 (s, 2 H), 7.20 (d, *J* = 5.4 Hz, 2 H), 7.00 (d, *J* = 7.7 Hz, 2 H), 6.68 (dd, *J* = 7.7, 5.6 Hz, 2 H), 5.98 (br s, 2 H), 2.22 (q, *J* = 7.6 Hz, 4 H), 1.65 (s, 18 H), 1.40 (s, 18 H), 0.93 (t, *J* = 7.6 Hz, 6 H)
Ru(4-EtPy)$_2$(DTBDiox)$_2$	7.78 (d, *J* = 2.1 Hz, 2 H), 7.21 (d, *J* = 6.6 Hz, 4 H), 6.60 (d, *J* = 6.6 Hz, 4 H), 5.94 (br s, 2 H), 2.45 (q, *J* = 7.6 Hz, 4 H), 1.66 (s, 18 H), 1.42 (s, 18 H), 0.99 (t, *J* = 7.6 Hz, 6 H)
Ru(4-BuPy)$_2$(DTBDiox)$_2$	8.33 (d, *J* = 2.1 Hz, 2 H), 7.37 (d, *J* = 6.6 Hz, 4 H), 6.15 (d, *J* = 2.1 Hz, 2 H), 6.09 (d, *J* = 6.6 Hz, 4 H), 2.03 (s, 18 H), 1.44 (s, 18 H), 0.39 (s, 18 H)
Ru(3-ClPy)$_2$(TBDiox)$_2$	7.64 (d, *J* = 2.1 Hz, 2 H), 7.53 (d, 2.2 Hz, 2 H), 7.50 (d, *J* = 8.8 Hz, 2 H), 7.43 (dd, *J* = 5.6, 1.0 Hz, 2 H), 6.80 (d, *J* = 5.7 Hz, 2 H), 6.78 (d, *J* = 5.9 Hz, 2 H), 6.27 (dd, *J* = 8.8, 2.2 Hz, 1.5 H), 6.18 (dd, *J* = 8.8, 2.2 Hz, 0.5 H), 1.38 (s, 18 H)
Ru(4-PhPy)$_2$(TBDiox)$_2$	7.75 (m, 2 H), 7.60 (m, 2 H), 7.34–7.26 (m, 14 H), 7.04 (m, 4 H), 6.09 (dd, *J* = 8.7, 2.1, 1.2 H), 5.99 (dd, *J* = 8.7, 2.1 Hz, 0.8 H), 1.44 (s, 18 H)
Ru(4-VPy)$_2$(TBDiox)$_2$	7.72 (m, 2 H), 7.52 (m, 2 H), 7.16 (m, 4 H), 6.78 (m, 4 H), 6.37 (dd, *J* = 17.6, 10.8 Hz, 2 H), 6.05 (dd, *J* = 8.7, 2.2 Hz, 1 H), 5.95 (dd, *J* = 8.7, 2.2 Hz, 1 H), 5.65 (d, *J* = 17.6 Hz, 2 H), 5.31 (d, *J* = 10.8 Hz, 2 H), 1.45 (s, 18 H)

[a] Obtained at 300 MHz in $CDCl_3$ solution. The chemical shifts are reported in parts per million (δ) downfield from tetramethylsilane. Key: s = singlet; d = doublet; t = triplet; q = quartet; m = multiplet.

Table II. ESR Data for [Cp$_2$Co]-*t*-[Ru(RPy)$_2$(R′Diox)$_2$],[a] R1

	g_1	g_2[b]	g_3
[Cp$_2$Co][Ru(3-AcPy)$_2$(DTBDiox)$_2$]	2.32	2.12 (176)	*c*
[Cp$_2$Co][Ru(4-AcPy)$_2$(DTBDiox)$_2$]	2.34	2.11 (175)	1.91
[Cp$_2$Co][Ru(3-ClPy)$_2$(DTBDiox)$_2$]	2.31	2.15 (69)	1.82
[Cp$_2$Co][Ru(3-ClPy)$_2$(DTBDiox)$_2$][d]	2.30	2.15	1.80
[Cp$_2$Co][Ru(4-ClPy)$_2$(DTBDiox)$_2$]	2.31	2.15 (100)	1.82
[Cp$_2$Co][Ru(3-PhPy)$_2$(DTBDiox)$_2$]	2.36	2.15 (94)	2.01
[Cp$_2$Co][Ru(Py)$_2$(DTBDiox)$_2$]	2.35	2.16 (103)	1.82
[Cp$_2$Co][Ru(4-PhPy)$_2$(DTBDiox)$_2$]	2.34	2.16 (84)	1.81
[Cp$_2$Co][Ru(4-VPy)$_2$(DTBDiox)$_2$]	2.35	2.16 (85)	1.86
[Cp$_2$Co][Ru(4-MePy)$_2$(DTBDiox)$_2$]	2.22	2.16 (120)	1.87
[Cp$_2$Co][Ru(3-EtPy)$_2$(DTBDiox)$_2$]	2.34	2.16 (98)	1.78
[Cp$_2$Co][Ru(4-EtPy)$_2$(DTBDiox)$_2$]	2.34	2.18 (130)	1.77
[Cp$_2$Co][Ru(4-BuPy)$_2$(DTBDiox)$_2$]	2.30	2.18 (110)	1.77
[Cp$_2$Co][Ru(3-ClPy)$_2$(TBDiox)$_2$]	2.36	2.17 (117)	1.80
[Cp$_2$Co][Ru(4-PhPy)$_2$(TBDiox)$_2$]	2.35	2.18 (74)	*c*
[Cp$_2$Co][Ru(4-VPy)$_2$(TBDiox)$_2$]	2.36	2.18 (70)	*c*

[a] Samples were prepared in situ by addition of a solution of Cp$_2$Co in DCE to the solid starting material. Spectra were recorded at 110–115 K. [b] Peak-peak separation (*G*) in parentheses. [c] Due to broadness g_3 is undefined. [d] Solid state data at 77 K.

Couple IV is normally quasi-reversible or approaching irreversibility ($i_c/i_a > 1$) but always has a clear return wave. Coulometry was carried out for some couples. On the basis of this and similarities in current from one couple to another, all the redox processes involve one electron.

The R1 and O1 species may also be generated by bulk electrolysis or by chemical reduction or oxidation respectively. These processes are fully reversible. The O2 species is unstable on the controlled-potential time scale, and attempts to generate it by bulk electrolysis resulted in some decomposition. Attempts to generate R2 by similar methods resulted in completely irreversible changes.

Fourier Transform Infrared Spectra. FTIR data were collected for most of the S and O1 complexes (supplementary data, Tables SIII and SIV) and for [Cp$_2$Co][Ru(3-ClPy)$_2$(DTBDiox)$_2$], the only isolated R1 material. Spectra of the O1 species were recorded as Nujol or HCBD mulls since KBr reduces these complexes.

The spectrum of [Cp$_2$Co][Ru(3-ClPy)$_2$(DTBDiox)$_2$] shows prominent absorptions at 1414, 1404, 1281, and 1237 cm^{-1}. The FTIR spectra of the S species are distinguished by intense absorptions around 1150 cm^{-1}, which are unique to this redox level. The spectra of the O1 species are dominated by counterion absorptions, with other strong bands around 1600 (4-RPy), 1450, 1420, 1370, and 1240 cm^{-1}.

Photoelectron Spectra. Data for the Ru(3d$_{5/2}$) and for the core levels of oxygen and nitrogen are given in Table V.

Electronic Spectra. Solution electronic spectroscopic data for the R1, S, and O1 species are collected in Tables VI–VIII, and typical spectra are displayed in Figure 4. Representative S and O1 spectra were also obtained in the solid state (as Nujol mulls); these showed no significant differences from the solution data.

Discussion

Stereochemistry. In the *t*-Ru(RPy)$_2$(DTBDiox)$_2$ complex geometry, two 3,5-di-*tert*-butyldioxolene ligands can theoretically give rise to two isomers, one each of C_{2v} and C_{2h} symmetry, depending on the relative orientations of the *tert*-butyl groups (and assuming axial trans ligands). The NMR spectra indicate that only one isomer is formed, and the temperature invariance of these spectra suggests that isomerization does not occur in the temperature range studied. Careful spectroscopic and chromatographic examination of the mother liquors from which these complexes were isolated gave no evidence of a second isomer. This, in concert with the arguments below, suggests that for the bis(3,5-di-*tert*-butyldioxolene) complexes only one trans isomer is formed in the synthetic procedure. Trans to cis isomerization occurs at higher temperatures.[12]

Single-crystal X-ray data for *t*-Ru(4-BuPy)$_2$(DTBDiox)$_2$ and *t*-[Ru(3-ClPy)$_2$(DTBDiox)$_2$]PF$_6$ establishes that the solid state geometry is C_{2h}.[7,16,17] Assuming that the solid-state and solution structures are the same, the absence of the C_{2v} isomer may be attributed to an unfavorable steric interaction between the two cis *tert*-butyl substituents in this geometry. Support for this analysis derives from studies of the corresponding monosubstituted,

Table III. ESR Data for *t*-$[Ru(RPy)_2(R'Diox)_2]^+$, O1, Salts

	frozen solution[a,b,e]		solid state[a,e]	
	$g_\perp$	$g_\parallel$	$g_\perp$	$g_\parallel$
$[Ru(3\text{-}AcPy)_2(DTBDiox)_2]PF_6$	2.01[d] (130)		1.98[d] (84)	2.09
$[Ru(4\text{-}AcPy)_2(DTBDiox)_2]PF_6$	2.00[d] (115)		1.98[d] (74)	2.10
$[Ru(3\text{-}ClPy)_2(DTBDiox)_2]ClO_4$	2.00[c] (110)		1.99[d] (88)	2.07
$[Ru(3\text{-}ClPy)_2(DTBDiox)_2]SO_3CF_3$	2.01[c] (87)		1.99[c] (50)	2.07
$[Ru(4\text{-}ClPy)_2(DTBDiox)_2]PF_6$	2.00[d] (157)		1.99[d] (145)	2.10
$[Ru(3\text{-}PhPy)_2(DTBDiox)_2]PF_6$	2.01[d] (153)		1.98[d] (104)	2.10
$[Ru(Py)_2(DTBDiox)_2]PF_6$	1.99[d] (166)		1.97[d] (100)	2.07
$[Ru(4\text{-}PhPy)_2(DTBDiox)_2]SO_3CF_3$	1.98[d] (123)	2.14	1.97[c] (53)	2.12
$[Ru(4\text{-}VPy)_2(DTBDiox)_2]PF_6$	1.99[d] (122)	2.09	1.98[d] (95)	2.08
$[Ru(4\text{-}MePy)_2(DTBDiox)_2]ClO_4$	2.01[d] (190)		1.97[c] (53)	2.10
$[Ru(4\text{-}MePy)_2(DTBDiox)_2]SO_3CF_3$	2.01[c] (140)		1.96[c] (43)	2.16
$[Ru(3\text{-}EtPy)_2(DTBDiox)_2]PF_6$	2.01[d] (150)		1.99[d] (92)	2.10
$[Ru(4\text{-}EtPy)_2(DTBDiox)_2]PF_6$	2.01[d] (147)		1.99[d] (108)	2.08
$[Ru(4\text{-}BuPy)_2(DTBDiox)_2]SO_3CF_3$	2.00[c] (135)		1.98[c] (35)	2.03
$[Ru(3\text{-}ClPy)_2(TBDiox)_2]PF_6$	2.01[c] (120)		1.99[c] (115)	2.10
$[Ru(4\text{-}PhPy)_2(TBDiox)_2]PF_6$	2.01[d] (210)		1.96[d] (120)	2.17
$[Ru(4\text{-}VPy)_2(TBDiox)_2]PF_6$	2.01[d] (208)		2.01[d] (290)	

[a] A single value is an unresolved signal probably closely associated with $g_\perp$. [b] Solvent DCE. [c] 77 K. [d] 115 K. [e] Peak-peak separations (*G*) in parentheses.

Table IV. Electrochemical Data for *t*-$Ru(RPy)_2(R'Diox)_2$ Complexes[a]

complex	$E_{1/2}$ vs SCE, V				
	I[b]	II	III	IV	
	O2	O1	S	R1	R2
$Ru(3\text{-}AcPy)_2(DTBDiox)_2$	+1.11	+0.32	−0.57	−1.50	qr[c]
$Ru(4\text{-}AcPy)_2(DTBDiox)_2$	+1.08	+0.34	−0.55	−1.27	qr
$Ru(3\text{-}ClPy)_2(DTBDiox)_2$	+1.08	+0.30	−0.60	−1.51	qr
$Ru(4\text{-}ClPy)_2(DTBDiox)_2$	+1.11	+0.29	−0.62	−1.59	ir
$Ru(3\text{-}PhPy)_2(DTBDiox)_2$	+1.11	+0.26	−0.63	−1.63	ir
$Ru(Py)_2(DTBDiox)_2$	+1.07	+0.25	−0.65	−1.63	ir
$Ru(4\text{-}PhPy)_2(DTBDiox)_2$	+1.07	+0.24	−0.66	−1.56	ir
$Ru(4\text{-}VPy)_2(DTBDiox)_2$	+1.07	+0.24	−0.66	−1.55	qr
$Ru(4\text{-}MePy)_2(DTBDiox)_2$	+1.05	+0.24	−0.67	−1.72	ir
$Ru(3\text{-}EtPy)_2(DTBDiox)_2$	+1.08	+0.23	−0.68	−1.69	ir
$Ru(4\text{-}EtPy)_2(DTBDiox)_2$	+1.06	+0.23	−0.68	−1.71	ir
$Ru(4\text{-}BuPy)_2(DTBDiox)_2$	+1.07	+0.23	−0.68	−1.70	ir
$Ru(3\text{-}ClPy)_2(TBDiox)_2$	+1.20	+0.41	−0.41	−1.34	qr
$Ru(4\text{-}PhPy)_2(TBDiox)_2$	+1.14	+0.34	−0.50	−1.47	qr
$Ru(4\text{-}VPy)_2(TBDiox)_2$	+1.15	+0.35	−0.51	−1.46	
$Ru(4\text{-}BuPy)_2(TBDiox)_2$	+1.12	+0.36	−0.50	−1.56	ir
$Ru(4\text{-}BuPy)_2(MeDiox)_2$	+1.12	+0.36	−0.49	−1.55	ir
$Ru(4\text{-}BuPy)_2(Diox)_2$	+1.25	+0.44	−0.45	−1.57	qr
$Ru(4\text{-}BuPy)_2(ClDiox)_2$	+1.35	+0.61	−0.28	−1.44	qr

[a] Measurements were made by using 1,2-dichloroethane solutions of the starting materials ($\sim 10^{-3}$ M) containing ~0.2 M TBAP or TBA-H. $E_{1/2}$ values are obtained from cyclic voltammetry at 100 mV s^{-1}. [b] DTBDiox complexes showed a third oxidation process with E_{pa} between +1.7 and +2.0 V, appearing as a shoulder close to the solvent limit and having no cathodic peak. [c] Key: qr = quasi-reversible; ir = irreversible.

4-*tert*-butyldioxolene complexes. In these cases, neither trans isomer is likely to be sterically constrained, and ^1H NMR data indicate the presence of two isomers. The relative proportions of the two isomers vary (Table I); $Ru(4\text{-}VPy)_2(TBDiox)_2$ and $Ru(4\text{-}PhPy)_2(TBDiox)_2$ give the two isomers in approximately equal concentrations, whereas $Ru(3\text{-}ClPy)_2(TBDiox)_2$ gives an isomer ratio of approximately 3:1.

Electronic Structure. Each of the starting materials gives rise to five redox products as established by cyclic voltammetry (Table IV). *c*-[12] and *t*-$Ru(RPy)_2(R'Diox)_2$ analogues give distinct, though very similar, cyclic voltammograms. This and the reversibility of the spectroelectrochemical experiments for the trans species suggest that no structural changes occur during the redox processes generating O1 and R1, though some decomposition is evident on the longer time scale for O2 and R2.

As discussed previously for the $Ru(bpy)(R'Diox)_2$ complexes,[9] the electronic structures of the various redox products are not obvious from their molecular formulas. Critical evaluation of the

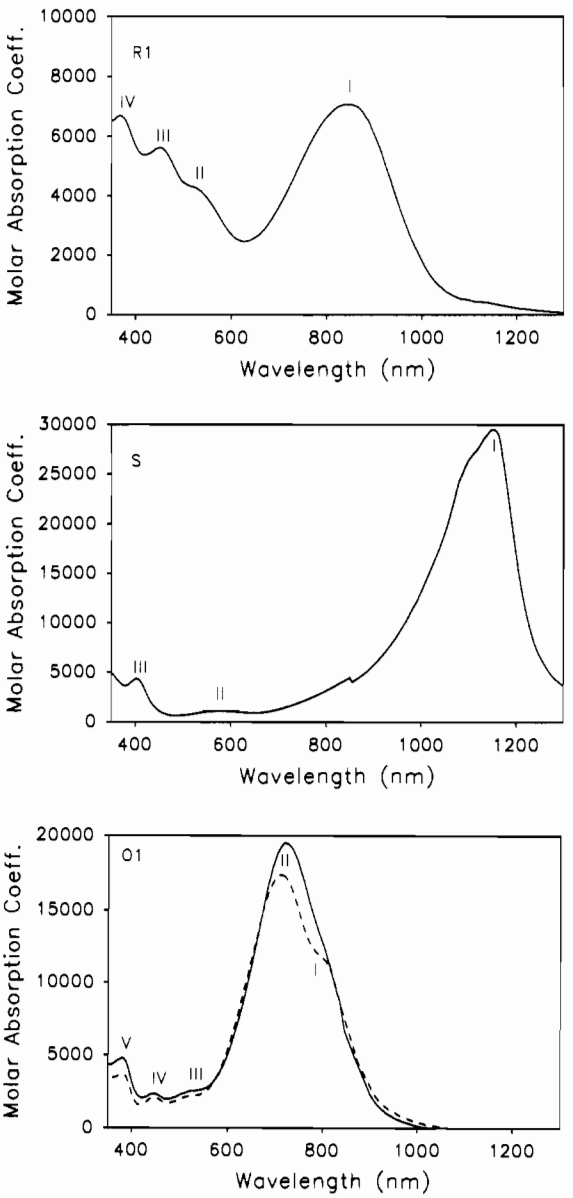

Figure 4. Visible–near-IR spectra in DCE solution of (top) R1 $[Ru(3\text{-}ClPy)_2(TBDiox)_2]^-$ generated electrochemically, (middle) S $Ru(Py)_2(DTBDiox)_2$, and (bottom) O1 $[Ru(3\text{-}AcPy)_2(DTBDiox)_2]PF_6$ (—) and $[Ru(3\text{-}EtPy)_2(DTBDiox)_2]PF_6$ (---). The discontinuity around 850 nm in the S spectrum is an instrumental artifact.

Table V. Photoelectron Emission Data (eV)[a]

complex	Ru($3d_{5/2}$)	O(1s)[b]	N(1s)[b]
R1			
$[Cp_2Co][Ru(3\text{-}ClPy)_2(DTBDiox)_2]$	281.4[c]	528.2 (0.22) 529.9 (0.56) 531.3 (0.22)	399.2 (0.83) 397.7 (0.17)
S			
$Ru(3\text{-}ClPy)_2(DTBDiox)_2$	280.8	530.8 (0.47) 532.2 (0.33) 533.5 (0.20)	400.3 (0.76) 401.3 (0.24)
$Ru(Py)_2(DTBDiox)_2$	281.0	*d*	400.4 (0.79) 399.6 (0.21)
$Ru(4\text{-}BuPy)_2(DTBDiox)_2$	280.9	*d*	400.3 (0.71) 399.3 (0.29)
O1			
$[Ru(3\text{-}ClPy)_2(DTBDiox)_2]ClO_4$	281.8	*d*	400.5
$[Ru(4\text{-}MePy)_2(DTBDiox)_2]ClO_4$	281.9	530.6 (0.27) 531.8 (0.45) 533.1 (0.24) 534.3 (0.04)	399.3 (1.0)

[a] Standardized to C(1s) at 285 eV. Errors vary between runs from ±0.1 to ±0.3 eV. [b] Relative intensities of Gaussian components are given in parentheses. [c] Average of two runs; data may be suspect due to charging problems. [d] Contaminated with silicone grease.

Table VI. Electronic Spectroscopic Data for *t*-$[Ru(RPy)_2(R'Diox)_2]^-$, R1, Complexes

complex	λ_{max}/nm (approx log ϵ)[a] (R1,I)	(R1,II)	(R1,III)	(R1,IV)	conditions
$[Ru(3\text{-}AcPy)_2(DTBDiox)_2]^-$	840 (3.85)	br	450 (3.67)	372	TBAH/DCE
	845	br	450 sh		Cp_2Co/DCE
$[Ru(3\text{-}ClPy)_2(DTBDiox)_2]^-$	*b*	545 (3.52)	457 (3.56)	368	TBAH/DCE
	865	534	450		Cp_2Co/DCM
$[Ru(4\text{-}ClPy)_2(DTBDiox)_2]^-$	*b*	532 (3.43)	444 sh	365 (3.81)	TBAP/DCE
	835				Cp_2Co/DCE
$[Ru(3\text{-}PhPy)_2(DTBDiox)_2]^-$	845 (3.78)	520 sh	450 sh	360 sh	TBAH/DCE
	820				Cp_2Co/DCE
$[Ru(Py)_2(DTBDiox)_2]^-$	825 (3.85)	484 sh	400 (3.62)	350 sh	TBAH/DCE
	814				Cp_2Co/DCE
$[Ru(4\text{-}PhPy)_2(DTBDiox)_2]^-$	*b*	587	465	375	TBAP/DCE
	836	574	480		Cp_2Co/DCE
$[Ru(4\text{-}VPy)_2(DTBDiox)_2]^-$	*b*	608 (3.64)	486 (3.62)	380 (3.84)	TBAH/DCE
	845	620	492	380 sh	Cp_2Co/DCE
$[Ru(4\text{-}MePy)_2(DTBDiox)_2]^-$	806 (3.89)	476 sh			Cp_2Co/DCE
$[Ru(3\text{-}EtPy)_2(DTBDiox)_2]^-$	830 (3.80)	492 (3.50)	398 sh	354 sh	TBAH/DCE
	811	495 sh			Cp_2Co/DCE
$[Ru(4\text{-}EtPy)_2(DTBDiox)_2]^-$	*b*	494 sh	397 (3.65)		TBAP/DCE
	807 (3.90)	476 sh			Cp_2Co/DCE
$[Ru(4\text{-}BuPy)_2(DTBDiox)_2]^-$	804	497		303	TBAP/DCE
	804 (3.82)	486 sh			Cp_2Co/DCE
$[Ru(3\text{-}ClPy)_2(TBDiox)_2]^-$	850 (3.81)	516 sh	450 (3.65)	360 (3.70)	TBAH/DCE
$[Ru(4\text{-}PhPy)_2(TBDiox)_2]^-$	802 (3.84)	540	500 sh		Cp_2Co/DCE
$[Ru(4\text{-}VPy)_2(TBDiox)_2]^-$	804 (3.81)	sh	488		Cp_2Co/DCE
$[Ru(4\text{-}BuPy)_2(Diox)_2]^-$	750	470 sh	407	301	TBAP/DCE
$[Ru(4\text{-}BuPy)_2(ClDiox)_2]^-$	741	463 sh	412	307	TBAP/DCE

[a] Samples were prepared in situ by the addition of Cp_2Co to solutions of the corresponding starting materials or by bulk electrolysis of the starting materials in DCE solutions that were approximately 0.5 M in TBAH or TBAP. Some differences in the low-energy peak positions are observed for the same species generated by the two methods. This is probably due to ion-pairing effects. Key: sh = shoulder.

Chart II

R2	$[Ru^{II}(bpy)(cat)_2]^{2-}$	
R1	$[Ru^{III}(bpy)(cat)_2]^-$	$\leftrightarrow [Ru^{II}(bpy)(cat)(sq)]^-$
S	$Ru^{II}(bpy)(sq)_2$	$\leftrightarrow Ru^{III}(bpy)(cat)(sq)$
O1	$[Ru^{II}(bpy)(q)(sq)]^+$	$\leftrightarrow [Ru^{III}(bpy)(sq)_2]^+$
O2	$[Ru^{II}(bpy)(q)_2]^{2+}$	

possible electronic structures gave the valence bond descriptions in Chart II for the various redox species for $[Ru(bpy)(R'Diox)_2]^{z+}$ based upon their chemical and physical properties; the first canonical form is believed to be the dominant one. Mixed valence species are delocalized.

The electronic structures required to describe the R1, S, and O1 species were reconciled by a simple molecular orbital model, involving the three ruthenium d (t_{2g} in O_h symmetry) and the dioxolene $3b_1$ (in C_{2v} symmetry) orbitals, which all mix extensively.

Neglecting the ligand substituents, the trans complexes have D_{2h} symmetry. The $3b_1$ (in local C_{2v} symmetry) orbitals[19] of the two dioxolene ligands transform as $b_{1u} + b_{2g}$. The t_{2g} (in local O_h symmetry) orbitals of the central ruthenium atom transform as $a_g + b_{2g} + b_{3g}$. Within this model, the ligand and metal valence orbitals of b_{2g} symmetry mix, while the remaining ligand and metal valence levels remain essentially unmixed. An effective oxidation state of the ruthenium may be calculated by summing the percentage of metal character of each orbital multiplied by its occupancy. The dioxolene lone-pair and pyridine π^* levels are also relevant to a full spectroscopic analysis of these species (Figure 5). The electrochemical and spectroscopic data, for the various redox products, are interpreted in the light of this model by using methods discussed in detail elsewhere.[6,8,9]

R2 Species. In the R2 products, the five valence orbitals are occupied by ten electrons, six from the central ruthenium ion and two from each dioxolene ligand. Thus, regardless of the relative

(19) Gordon, D. J.; Fenske, R. F. *Inorg. Chem.* **1982**, *21*, 2907, 2916.

Table VII. Electronic Spectroscopic Data for *t*-Ru(RPy)$_2$(R'Diox)$_2$, S, Complexes

complex	λ_{max}/nm (approx log ϵ)[b] (S,I)	(S,II)	(S,III)	(S,IV)	solvent
Ru(3-AcPy)$_2$(DTBDiox)$_2$	1155 (4.48) 1110 sh	585 (3.09)	395 (3.69)	318 sh[a]	DCB
Ru(3-ClPy)$_2$(DTBDiox)$_2$	1160 (4.54) 1110 sh	584 (3.01)	400 sh 371 (3.71)	320 sh[a]	DCB
Ru(4-ClPy)$_2$(DTBDiox)$_2$	1160 1110 sh	576	406 367	318 sh[a]	DCB
Ru(3-PhPy)$_2$(DTBDiox)$_2$	1153 (4.51) 1110 sh	580 (3.07)	408 (3.68) 360 sh	320 sh[a]	DCB
Ru(Py)$_2$(DTBDiox)$_2$	1155 (4.47) 1100 sh	580 (3.05)	403 (3.64)	324 (3.84)	DCE
Ru(4-PhPy)$_2$(DTBDiox)$_2$	1160 (4.56) 1110 sh	576 (3.10)	450 sh 380 (3.88)	320 sh[a]	DCB
Ru(4-VPy)$_2$(DTBDiox)$_2$	1163 (4.68) 1115 sh	574 (3.23)	450 sh 397 (3.87)	316[a]	DCB
Ru(4-MePy)$_2$(DTBDiox)$_2$	1160 (4.56) 1105 sh	575 (3.06)	402 (3.58)	326[a]	DCB
Ru(3-EtPy)$_2$(DTBDiox)$_2$	1165 (4.59) 1110 sh	574 (3.06)	404 (3.63)	325[a]	DCB
Ru(4-EtPy)$_2$(DTBDiox)$_2$	1160 (4.59) 1110 sh	572 (3.10)	400 (3.64)	323[a]	DCB
Ru(4-BuPy)$_2$(DTBDiox)$_2$	1160 (4.55) 1110 sh	577 (3.04)	400 (3.58)	324 (3.61)	DCE
Ru(3-ClPy)$_2$(TBDiox)$_2$	1165 (4.53) 1115 sh	575 (3.04)	402 (3.65) 372 sh		DCB
Ru(4-PhPy)$_2$(TBDiox)$_2$	1165 (4.52) 1115 sh	582 (3.05)	400 sh 366 sh	320 sh	DCE
Ru(4-VPy)$_2$(TBDiox)$_2$	1165 (4.55) 1115 sh	576 (3.04)	454 sh 380 (3.80)		DCB
Ru(4-BuPy)$_2$(TBDiox)$_2$	1161 (4.69) 1110 (4.67)	567 (3.04)	390 (3.64)	323 (3.98)	DCE
Ru(4-BuPy)$_2$(MeDiox)$_2$	1155 (4.46) 1102 (4.43)	562 (2.90)	388 sh	323 (3.81)	DCE
Ru(4-BuPy)$_2$(Diox)$_2$	1132 (4.47) 1080 (4.46)	560 (3.04)	386 sh	315 (4.0)	DCE
Ru(4-BuPy)$_2$(ClDiox)$_2$	1144 (4.38) 1088 sh	563 (2.98)	393 sh	324 sh	DCE

[a] Observed in DCE solution. [b] Key: sh = shoulder.

Table VIII. Electronic Spectroscopic Data for *t*-[Ru(RPy)$_2$(R'Diox)$_2$]$^+$, O1, Complexes[a]

complex	λ_{max}/nm (approx log ϵ) (O1,I)	(O1,II)	(O1,III)	(O1,IV)	(O1,V)	solvent
[Ru(3-AcPy)$_2$(DTBDiox)$_2$]$^+$		721 (4.29)	520 sh	448 (3.37)	382 (3.68)	DCE
[Ru(4-AcPy)$_2$(DTBDiox)$_2$]$^+$		726 (4.23)	532 sh	450 (3.42)	378	DCE
[Ru(3-ClPy)$_2$(DTBDiox)$_2$]$^+$		720 (4.27)	530 sh	450 (3.36)	381 (3.71)	DCE
[Ru(4-ClPy)$_2$(DTBDiox)$_2$]$^+$		721 (4.20)	536 sh	450 (3.26)	374 (3.60)	DCE
[Ru(3-PhPy)$_2$(DTBDiox)$_2$]$^+$	800 sh	717 (4.17)	520 sh	448 (3.28)	380 (3.59)	DCE
[Ru(Py)$_2$(DTBDiox)$_2$]$^+$	805 sh	716 (4.26)	518 sh	450 (3.28)	380 (3.57)	DCE
[Ru(4-PhPy)$_2$(DTBDiox)$_2$]$^+$	820 sh	728 (4.25)	530 sh	450 sh	372 (3.78)	DCB
[Ru(4-VPy)$_2$(DTBDiox)$_2$]$^+$	816 sh	720 (4.12)	528 sh	450 (3.28)	380 sh	DCE
[Ru(4-MePy)$_2$(DTBDiox)$_2$]$^+$	818 sh	713 (4.14)	530 sh	450 (3.29)	384 (3.51)	DCE
[Ru(3-EtPy)$_2$(DTBDiox)$_2$]$^+$	800 sh	710 (4.24)	520 sh	446 (3.35)	380 (3.58)	DCE
[Ru(4-EtPy)$_2$(DTBDiox)$_2$]$^+$	798 sh	711 (4.08)	520 sh	448 (3.21)	383 (3.45)	DCE
[Ru(4-BuPy)$_2$(DTBDiox)$_2$]$^+$	810 sh	710 (4.19)	526 sh	446 (3.30)	383 (3.54)	DCE
[Ru(3-ClPy)$_2$(TBDiox)$_2$]$^+$		722 (4.12)	536 sh	444 (3.11)	368 (3.48)	DCE
[Ru(4-PhPy)$_2$(TBDiox)$_2$]$^+$	800 sh	712 (4.04)		440 sh	370 sh	DCM
[Ru(4-VPy)$_2$(TBDiox)$_2$]$^+$	796 sh	716 (4.22)	528 sh	438 sh	366 sh	DCE
[Ru(4-BuPy)$_2$(Diox)$_2$]$^+$	818	688	520 sh	440	374	DCE
[Ru(4-BuPy)$_2$(ClDiox)$_2$]$^+$	828	703	520 sh	436	395	DCE

[a] In general, spectra recorded in DCB show a red shift of between 5 and 15 nm in the low energy bands, compared with DCE or DCM. Key: sh = shoulder.

ordering or metal–ligand coefficients of the five valence orbitals, the only possible electronic description for the R2 complexes is [Ru^{II}(RPy)$_2$(cat)$_2$]$^{2-}$. However, since these species are unstable, there is no experimental corroboration of this assignment.

R1 Species. The R1 complexes have a total of nine valence electrons, with one electron in the highest occupied molecular orbital (HOMO). The character of the HOMO defines the electronic description of these materials. A [Ru^{III}(RPy)$_2$(cat)$_2$]$^-$ structure results if the HOMO is predominantly metal, while a [Ru^{II}(RPy)$_2$(cat)(sq)]$^-$ structure pertains if the HOMO is predominantly ligand in character.

The various R1 *t*-[Ru(RPy)$_2$(R'Diox)$_2$]$^-$ species have ESR spectra (Table II) with two or three distinct *g* values, typical of low-spin d^5 Ru^{III}.[20-25] While the R1 [Ru(bpy)(R'Diox)$_2$]$^-$ species

(20) DeSimone, R. E. *J. Am. Chem. Soc.* **1973**, *95*, 6238.
(21) Sakaki, S.; Hagiwara, N.; Yanase, Y.; Ohyoshi, A. *J. Phys. Chem.* **1978**, *82*, 1917.
(22) Raynor, J. B.; Jeliazkowa, B. G. *J. Chem. Soc., Dalton Trans.* **1982**, 1185.
(23) Hudson, A.; Kennedy, M. J. *J. Chem. Soc. A* **1969**, 1116.
(24) Lahiri, G. K.; Bhattacharya, S.; Ghosh, B. K.; Chakravorty, A. *Inorg. Chem.* **1987**, *26*, 4324.

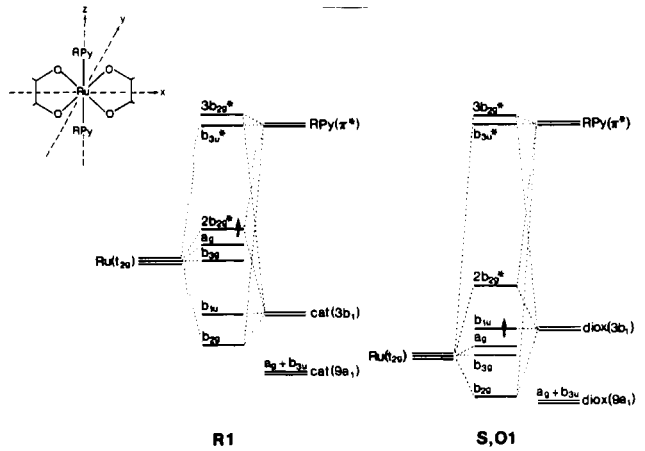

Figure 5. Qualitative molecular orbital diagrams for (left) R1, and (right) S and O1 species. These are based on group theory (D_{2h} symmetry) and the electronic spectra and are not to scale. The ordering of the MO's is probably the same for S and O1 though the relative energies and amount of mixing will differ somewhat. The singly occupied HOMO's in R1 and O1 are denoted by arrows. The O1 HOMO is doubly occupied in S. Ligand orbital symmetries are those given by Fenske.[19] The free-ligand lone-pair orbitals ($9a_1$) are indicated, but for simplicity they are not included in the MO's of the complex.

also show evidence for a Ru^{III} contribution,[9] it is certainly not so evident as in these *t*-bis(pyridine) species.

The Ru^{III} electronic structure requires that both dioxolene ligands be in the catechol oxidation state. This assignment is supported by the IR data for $[Cp_2Co][Ru(3\text{-}ClPy)_2(DTBDiox)_2]$ in which the two strongest bands are at 1237 and 1281 cm^{-1}. Coordinated catechols typically display one or two intense absorptions in the 1250-cm^{-1} region,[26-30] the more intense of which is normally attributed to the C–O stretching mode.

The PES $Ru(3d_{5/2})$ binding energy for $[Cp_2Co][Ru(3\text{-}ClPy)_2(DTBDiox)_2]$ (Table V) is 281.4 eV, in the range which may be associated with either Ru^{II} or Ru^{III}.[31-38] It is higher than the values observed for R1 species in the bipyridine series[9] and notably higher than the values for the S species. While the inner-shell binding energies of metals in complexes may be used to infer the oxidation state of the metal, the practice requires caution,[34] and comparisons are best made with complexes containing similar ligands. However the data are consistent with a Ru^{III} species bound to two strongly π-donating catecholate ligands.

Further support for the $[Ru^{III}(RPy)_2(cat)_2]^-$ structure comes from comparison of the shifts in the various redox potentials as a function of pyridine or dioxolene substituent (Figure 3). Couple IV is markedly dependent on pyridine substituent whereas couples I, II, and III vary very little, but show a much greater dependence on dioxolene substituent than does couple IV. This suggests that couple IV is metal-based ($Ru^{III/II}$) and couples I, II, and III are largely dioxolene ligand-based.

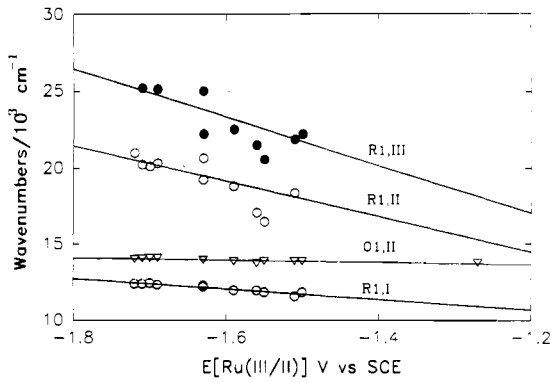

Figure 6. Plots showing the variation of selected charge-transfer bands with the $Ru^{III/II}$ potential, couple IV, for DTBDiox complexes. The linear regressions do not include the data for the 4-vinyl- and 4-phenylpyridine complexes.

Thus the data unequivocally support the formulation $[Ru^{III}(RPy)_2(cat)_2]^-$ and it remains to demonstrate that the electronic spectra (Figure 4; Table VI) can be assigned in this context. The HOMO, $2b_{2g}$*, is then mainly metal, and the lower energy electronic transitions will terminate thereon.

The lowest energy absorption (band (R1,I)) occurring between 800 and 850 nm is clearly attributable to a catechol (π) to ruthenium ($d\pi$) ligand to metal charge-transfer (LMCT) transition,[39] $b_{1u} \rightarrow 2b_{2g}$*, as seen in other catechol complexes containing reducible metal ions.[25,30,40-42] It shifts to the blue as the catechol becomes, upon substitution, a weaker donor, and shifts to the red with decreasing basicity of the pyridine ligand. Moreover band (R1,I) tracks the potential of the $Ru^{III/II}$ redox couple, IV, for the series of DTBDiox complexes. The correlation is linear, with a small negative slope (eq 1), i.e., a blue shift in the LMCT transition as the Ru^{III} species becomes more difficult to reduce (Figure 6).

$$\text{band (R1,I):}\quad \nu\ (cm^{-1}) = -3450E(Ru^{III/II}) + 6550 \quad (R = 0.95,\ 11\ \text{points}) \qquad (1)$$

Strictly, this type of correlation is only valid for a reversible redox couple, which is not the case for couple IV.[43] However the deviations from reversibility are not very large.

In the visible region, there are two absorptions (bands (R1,II,III) which might be attributed to pyridine (π) to Ru($d\pi$) LMCT transitions.[44] However, bands (R1,II,III) cannot be assigned in this manner since they both shift substantially to the red as the pyridine ligand becomes a better electron acceptor, and to the blue as R'Diox becomes a poorer donor. This behavior indicates metal to ligand charge transfer (MLCT) involving pyridine, a second cat → Ru($d\pi$) LMCT (from a lower catechol orbital), or possibly a cat → RPy ligand to ligand charge-transfer (LLCT) transition. The higher sensitivity of these bands to pyridine substitution relative to band (R1,I) and the lack of a second LMCT band in other catechol complexes[45,46] suggest that the LMCT assignment is not appropriate. We propose that these are MLCT transitions even though the metal is Ru^{III}. They occur in the visible region because of the very negative $Ru^{III/II}$ potential,

(25) Pell, S. D.; Salmonsen, R. B.; Abelleira, A.; Clark, M. J. *Inorg. Chem.* **1984**, *23*, 385.
(26) Wicklund, P. A.; Brown, D. G. *Inorg. Chem.* **1976**, *15*, 396.
(27) Brown, D. G.; Reinprecht, J. T.; Vogel, G. C. *Inorg. Nucl. Chem. Lett.* **1976**, *12*, 399.
(28) Brown, D. G.; Johnson, W. L. *Z. Naturforsch.* **1979**, *34B*, 712.
(29) Lynch, M. W.; Valentine, M.; Hendrickson, D. N. *J. Am. Chem. Soc.* **1982**, *104*, 6982.
(30) Hartmann, J. R.; Foxman, B. M.; Cooper, S. R. *Inorg. Chem.* **1984**, *23*, 1381.
(31) Weaver, T. R.; Meyer, T. J.; Adeyemi, S. A.; Brown, G. M.; Eckberg, R. P.; Hatfield, W. P.; Johnson, E. C.; Murray, R. W.; Untereker, D. *J. Am. Chem. Soc.* **1975**, *97*, 3039.
(32) Connor, J. A.; Meyer, T. J.; Sullivan, B. P. *Inorg. Chem.* **1979**, *18*, 1388.
(33) Feltham, R. D.; Brant, P. *J. Am. Chem. Soc.* **1982**, *104*, 641.
(34) Srivastava, S. *Appl. Spectrosc. Rev.* **1986**, *22*, 401.
(35) Geselowitz, D. A.; Kutner, W.; Meyer, T. J. *Inorg. Chem.* **1986**, *25*, 2015.
(36) Brant, P.; Stephenson, T. A. *Inorg. Chem.* **1987**, *26*, 22.
(37) Shepherd, R. E.; Proctor, A.; Henderson, W. W.; Myser, T. K. *Inorg. Chem.* **1987**, *26*, 2440.
(38) Gassman, P. G.; Winter, C. H. *J. Am. Chem. Soc.* **1988**, *110*, 6130.
(39) Lever, A. B. P. *Inorganic Electronic Spectroscopy*, 2nd ed.; Elsevier: Amsterdam, 1984.
(40) Salama, S.; Stong, J. D.; Neilands, J. B.; Spiro, T. G. *Biochemistry* **1978**, *17*, 3781.
(41) Bristow, S.; Enemark, J. H.; Garner, C. D.; Minelli, M.; Morris, G. A.; Ortega, R. B. *Inorg. Chem.* **1985**, *24*, 4070.
(42) Cox, D. D.; Benkovic, S. J.; Bloom, L. M.; Bradley, F. C.; Nelson, M. J.; Que, L., Jr.; Wallick, D. E. *J. Am. Chem. Soc.* **1988**, *110*, 2026.
(43) Dodsworth, E. S.; Lever, A. B. P. *Chem. Phys. Lett.* **1986**, *124*, 152.
(44) Clark, R. J. H.; Stead, M. J. *J. Chem. Soc., Dalton Trans.* **1981**, 1760.
(45) deLearie, L. A.; Haltiwanger, R. C.; Pierpont, C. G. *Inorg. Chem.* **1987**, *26*, 817.
(46) deLearie, L. A.; Haltiwanger, R. C.; Pierpont, C. G. *J. Am. Chem. Soc.* **1989**, *111*, 4324.

IV. Two MLCT transitions to pyridine are allowed by symmetry (Figure 5), Ru(a_g,$2b_{2g}$*) → RPy(b_{3u}*). These are assigned to bands (R1,II) and (R1,III), respectively, as the latter is expected to be stronger due to better overlap. LLCT transitions, b_{2g} → b_{3u}* and b_{1u} → $3b_{2g}$*, may also contribute to intensity in this region.

For the DTBDiox complexes, both transitions (R1,II,III) track the $Ru^{III/II}$ potential with significantly larger negative slopes than for the 800-nm absorption (Figure 6). The correlations are rather scattered, probably because many of the transitions appear as shoulders whose true transition energies are difficult to define accurately. These transitions for the 4-vinyl- and 4-phenylpyridine complexes lie well below the correlation lines and are not included in the statistics in eqs 2 and 3. The extra red shift for these last

$$\text{band (R1,II):}\quad \nu\ (\text{cm}^{-1}) = -11700E(Ru^{III/II}) + 446 \quad (R = 0.95,\ 7\ \text{points}) \tag{2}$$

$$\text{band (R1,III):}\quad \nu\ (\text{cm}^{-1}) = -15700E(Ru^{III/II}) + 1870 \quad (R = 0.82,\ 7\ \text{points}) \tag{3}$$

two species results from conjugation of the pyridine π system with that of the substituent, which lowers the π* level while not affecting the donor properties of the pyridine ligand and thus lowers the MLCT energy. This is further evidence for the MLCT (or LLCT) assignment.

Note that it would be more appropriate to correlate the MLCT transitions with the $Ru^{IV/III}$ potentials, but these data are not available; there is little doubt however that the $Ru^{III/II}$ potential (IV) varies with pyridine substituent in a parallel manner to the $Ru^{IV/III}$ potential.[47]

Band (R1,IV) occurs in most cases as a shoulder on the rising ligand UV absorption, and its behavior with changing substituents is not clear. It is almost certainly a CT transition as the ligands do not absorb at this energy.

S Species. The single-crystal X-ray structure[7,16] of *t*-Ru(4-BuPy)$_2$(DTBDiox)$_2$ does not clearly define the electronic structure of this complex. The C–O bond lengths of coordinated dioxolenes are normally characteristic of the ligand oxidation state.[2,48] However, this species shows average dioxolene C–O bond lengths of about 1.32 Å, identical with those in Ru(bpy)(Diox)$_2$ and significantly longer than those usually associated with coordinated semiquinones (1.29 Å) but shorter than the 1.35–1.37 Å expected for coordinated catechols. Also similar to Ru(bpy)(Diox)$_2$, the dioxolene rings have only very slight quinonoid character. The two dioxolene ligands are equivalent, although thermal disorder cannot absolutely be ruled out.

The ruthenium–oxygen bond lengths average 1.994 Å, 0.05 Å shorter than the Ru–O bonds in $[Ru^{II}(bpy)_2(DTBSq)]^{+}$ [16] and also shorter than the 2.028 Å average Ru–O bond length of $[Ru^{III}(C_2O_4)_3]^{3-}$,[49] but longer than the average Ru–O distance of 1.97 Å in Ru(DTBDiox)$_3$.[11] The Ru–N bonds are 2.08 Å, longer than those in either $[Ru^{II}(bpy)_2(DTBSq)]^{+}$ or $[Ru(bpy)_3]^{2+}$.[16,50] These data are consistent with a $Ru^{III}(RPy)_2$(cat)(sq) delocalized mixed-valence electronic structure.

The electrochemical data also support this view. Although the HOMO in R1 has mainly metal character, the large variation in redox potential III with dioxolene substituent (and relatively small variation with pyridine substituent (Figure 3)) indicates that R1 and S differ by one dioxolene ligand-based electron in their electronic structures, giving $Ru^{III}(RPy)_2$(cat)(sq). However, the PES data (Table V) for several S complexes show Ru($3d_{5/2}$) binding energies well within the normal Ru^{II} range[31-38] and lower than that observed for $[Ru^{III}(3\text{-ClPy})_2(DTBDiox)_2]^{-}$. This observation rules out the possibility of Ru^{IV} but suggests that there is some contribution from a Ru^{II} canonical form, similar to the situation in Ru(bpy)(R′Diox)$_2$. The diamagnetism of the S complexes requires that the Ru^{III} and sq in the mixed-valence structure be strongly antiferromagnetically coupled.

As previously observed for *c*-Ru(bpy)(R′Diox)$_2$ and Ru(DTBDiox)$_3$ complexes,[9,11] the FTIR spectra of the *t*-S species containing DTBDiox are dominated by a strong absorption at about 1150 cm^{-1}, which is not typical of either catechol or semiquinone species,[26-30] though a similar band has been reported in a series of Cu^{II}–semiquinone complexes.[51] The intensity of this absorption is convincing evidence that, despite its unusual position, it is associated with a C–O stretching vibration of the dioxolene ligand. Other IR absorptions are fairly typical of coordinated semiquinone, and there is no evidence for localized cat and sq ligands on the vibrational time-scale.

A localized mixed-valence system, which is unlikely in view of the strong Ru^{III}–sq coupling, is expected to show a broad cat → sq transition in the near-IR region, as seen in analogous Cr, Fe, and Co complexes.[29,52,53] A band is observed in this region (see below) but it is extremely intense and narrow, indicative of strongly coupled, class III, mixed-valence behavior.[54] Strong coupling requires a strong interaction between the ligand and metal b_{2g} orbitals as the ligands are too far apart to overlap directly. The antibonding combination, $2b_{2g}$*, will be the lowest unoccupied molecular orbital (LUMO) (Figure 5). If this were mainly metal b_{2g}, then the formal structure would approach $Ru^{IV}(RPy)_2(cat)_2$, while if it were dominantly ligand, it would be $Ru^{II}(RPy)_2(sq)_2$; a 50-50 mixed orbital leads to a Ru^{III} electronic structure with fully delocalized ligands. Most of the experimental data indicate that the Ru^{III} formula is the closest to reality, but the PES and IR spectra suggest that there is some $Ru^{II}(RPy)_2(sq)_2$ character, and therefore we conclude that the LUMO b_{2g}* orbital has slightly more than 50% ligand character.

The electronic spectra (Figure 4) of these materials are dominated by the intense near-IR absorption (band (S,I)) centered at about 1150 nm. Unlike band (R1,I), this transition is essentially unaffected by changing the pyridine substituent. There is a small dependence (Table VII) upon dioxolene substituent, the band shifting to higher energy for the less electron-donating dioxolenes, in accordance with an LMCT dioxolene → Ru(dπ) assignment. This behavior is appropriate for a b_{1u} → $2b_{2g}$* excitation, which is a bis(dioxolene) transition with LMCT character developed to the extent that the b_{2g} orbital has metal character. Typically, the near-IR band has a high-energy shoulder that may be a vibronic band as the splitting is small, typically around 400 cm^{-1}, possibly corresponding to ν(Ru–O).

Since the HOMO is the filled b_{1u} orbital and the LUMO is the even $2b_{2g}$* orbital, few transitions are allowed in this system, accounting for the absence of strong bands in the visible region. The broad, weak absorption near 580 nm (band (S,II)) is affected by ligand substituents in a similar manner to the near-IR band. This may be the dioxolene n → π* transition, which occurs around 700 nm in free semiquinones.[55] The highest dioxolene lone-pair orbitals ($9a_1$ in the free ligand[19]) transform as $a_g + b_{3u}$ in D_{2h} symmetry. The 580-nm band is therefore assigned to b_{3u} → $2b_{2g}$*, which is overlap forbidden, explaining its weakness. Preliminary resonance Raman data show no involvement of the axial pyridine ligands in this transition.[56]

Bands (S,III) are assigned to Ru(dπ) → RPy(π*) MLCT transitions, which are expected in the near-UV region, higher in energy than in the R1 species because the available d electrons are stabilized in S. Two transitions are seen in this region for complexes with the more electron-withdrawing pyridine substituents and these transitions move to particularly low energy with the conjugated 4-phenyl and 4-vinyl substituents, as discussed above for R1. Preliminary resonance Raman data confirm the

(47) Lever, A. B. P. *Inorg. Chem.* **1990**, *29*, 1271.
(48) Buchanan, R. M.; Kessel, S. L.; Downs, H. H.; Pierpont, C. G.; Hendrickson, D. N. *J. Am. Chem. Soc.* **1978**, *100*, 7894.
(49) Faure, R.; Duc, G.; Deloume, J.-P. *Acta Crystallogr.* **1986**, *C42*, 982.
(50) Rillema, D. P.; Jones, D. S.; Levy, H. A. *J. Chem. Soc., Chem. Commun.* **1979**, 849.
(51) Thompson, J. S.; Calabrese, J. C. *Inorg. Chem.* **1985**, *24*, 3167.
(52) Buchanan, R. M.; Claflin, J.; Pierpont, C. G. *Inorg. Chem.* **1983**, *22*, 2552.
(53) Buchanan, R. M.; Pierpont, C. G. *J. Am. Chem. Soc.* **1980**, *102*, 4951.
(54) Robin, M. B.; Day, P. *Adv. Inorg. Chem. Radiochem.* **1967**, *10*, 248.
(55) Dodsworth, E. S.; Lever, A. B. P. *Chem. Phys. Lett.* **1990**, *172*, 151.
(56) Stufkens, D. J.; Lever, A. B. P. Work in progress.

Table IX. Summary of Electronic Transition Assignments

		R1 Complexes	
band (R1,I)	$b_{1u} \rightarrow 2b_{2g}^*$	$cat(\pi) \rightarrow Ru(d\pi)$	LMCT
band (R1,II)	$a_g \rightarrow b_{3u}^*$	$Ru(d\pi) \rightarrow RPy(\pi^*)$	MLCT
	$b_{2g} \rightarrow b_{3u}^*$	$cat(\pi) \rightarrow RPy(\pi^*)$?	LLCT
band (R1,III)	$2b_{2g}^* \rightarrow b_{3u}^*$	$Ru(d\pi) \rightarrow RPy(\pi^*)$	MLCT
band (R1,IV)	$b_{1u} \rightarrow 3b_{2g}^*$	$cat(\pi) \rightarrow Ru(d\pi)$?	LMCT
		$cat(\pi) \rightarrow RPy(\pi^*)$?	LLCT
		S Complexes	
band (S,I)	$b_{1u} \rightarrow 2b_{2g}^*$	$R'Diox(\pi^*) \rightarrow Ru(d\pi) + R'Diox(\pi^*)$	LMCT/IL[a]
band (S,II)	$b_{3u} \rightarrow 2b_{2g}^*$	$R'Diox(n) \rightarrow Ru(d\pi) + R'Diox(\pi^*)$	LMCT/IL
band (S,III)	$b_{2g},a_g \rightarrow b_{3u}^*$	$Ru(d\pi) \rightarrow RPy(\pi^*)$	MLCT
band (S,IV)		$R'Diox(\pi) \rightarrow R'Diox(\pi^*)$	IL
		O1 Complexes	
band (O1,I)	$b_{2g},b_{3g} \rightarrow b_{1u}$	$Ru(d\pi) \rightarrow sq(\pi^*)$	MLCT
band (O1,II)	$b_{1u} \rightarrow 2b_{2g}^*$	$sq(\pi^*) \rightarrow Ru(d\pi) + sq(\pi^*)$	LMCT/IL
band (O1,III)	$a_g \rightarrow b_{1u}$	$sq(n) \rightarrow sq(\pi^*)$	IL
band (O1,IV)	$b_{3u} \rightarrow 2b_{2g}^*$	$sq(n) \rightarrow Ru(d\pi) + sq(\pi^*)$	LMCT/IL
band (O1,V)	$sq(\pi) \rightarrow b_{1u}$	$sq(\pi) \rightarrow sq(\pi^*)$	IL

[a] Intraligand. The asterisk designation in column 2 refers to orbitals that are antibonding in the MO scheme for the complex (Figure 5). In column 3 the asterisk refers to free ligand orbitals. The semiquinone π ($3b_1$ in the free ligand) orbital, which is a π level in catechol and π^* in quinone, is regarded as π^* here in both S and O1.

involvement of pyridine in this region.[56] Band (S,IV), around 320 nm, varies little with pyridine substituent and is assigned to the dioxolene $\pi \rightarrow \pi^*$ transition (involving $2b_{2g}^*$), which occurs at 380 nm in most semiquinone complexes.[55]

O1 Species. X-ray analysis[17] of $[Ru(3\text{-}ClPy)_2(DTBDiox)_2]^+$ shows clearly that both dioxolene ligands are in the semiquinone oxidation state and therefore the metal is Ru^{III}. The average dioxolene C–O distance is 1.29 Å, which is typical of semiquinones.[2,48] The Ru–O and Ru–N distances are both slightly longer than those in the S species, and the dioxolenes clearly have quinonoid character. The increase in metal–ligand bond lengths may be due to loss of π-back-bonding capability which exists in S because of the Ru^{II} character.

The $[Ru^{III}(RPy)_2(sq)_2]^+$ configuration is confirmed by the electrochemical and spectroscopic data. The shifts in couple II as functions of pyridine or dioxolene substituent (Figure 3) suggest that the redox process involves a largely dioxolene orbital, i.e., the b_{1u} LUMO. The PES $Ru(3d_{5/2})$ binding energies for those O1 complexes measured lie on the boundary between normal Ru^{II} and Ru^{III} [31-38] and are higher than those of the S and R1 complexes. Moreover, the FTIR spectra are typical of coordinated semiquinones, having no clearly identifiable ν(C–O), neither around 1650 (q) nor 1250 cm^{-1} (cat)[26-30] nor at 1150 cm^{-1} as in S. The strongest bands in the spectra are pyridine vibrations around 1600 cm^{-1}, in some species, and the bands around 1450 cm^{-1}, where ν(C–O) and a number of other vibrations are expected.

All the O1 species show one unpaired electron as indicated by magnetism or ESR studies. Frozen solutions of most O1 complexes give asymmetric ESR signals with only one g value resolved, this being close to the free-radical value of 2. However, two g values are resolved for all complexes in the solid state and two in frozen solution. The degree of anisotropy is small, similar to that observed in $[Ru(bpy)_2(sq)]^+$, $[Ru(bpy)(diox)_2]^+$, and a range of ligand-centered radical complexes of the $[Ru(bpy)_2]^{2+}$ fragment.[6,9,57-59] While other solid-state effects cannot be neglected, it is likely that exchange narrowing allows the resolution of the two intrinsic g values that cause the asymmetry of the other signals. Splitting of this type, $g_\perp < g_\parallel$, has previously been taken as an indication of some Ru^{III} contribution to the electronic ground state of Ru^{II}–semiquinone complexes.[6,9]

From the MO picture in Figure 5, it can be seen that the Ru^{III} configuration results from strong mixing of the metal and ligand b_{2g} orbitals to give b_{2g} and $2b_{2g}^*$ MO's, which each have about 50% metal character. The coupling is then to both equivalent semiquinone ligands leaving one unpaired electron distributed, in the b_{1u} orbital, over both semiquinones. The anisotropy seen in the ESR spectra then comes from mixing of a higher excited state which has the unpaired electron on the metal center.

The electronic spectra are also consistent with this MO description. The intense low energy electronic transition, occurring between 700 and 830 nm, band (O1,I,II) (Figure 4, Table VIII) is composite, being a strong band with a lower energy shoulder or peak. The higher energy component, band (O1,II), behaves very much like band (S,I) but with small dependences on both pyridine and dioxolene substituents (Figure 6). The substituent effects are in accord with assignment, as for (S,I), to the transition $b_{1u} \rightarrow 2b_{2g}^*$, which is intraligand with some LMCT character. It is broader than band (S,I) because the acceptor orbital has more antibonding character. For DTBDiox species:

$$\text{band (O1,II):}\quad \nu\ (cm^{-1}) = -735E(Ru^{III/II}) + 12800 \qquad (R = 0.80,\ 12\ \text{points}) \tag{4}$$

The lower energy component (O1,I) also shifts to a small degree with pyridine substituent, in the opposite direction to band (O1,II), and falls under band (O1,II), for pyridines with electron-withdrawing substituents. Since band (O1,I) usually appears as a shoulder, it gives a very scattered correlation when plotted against the $Ru^{III/II}$ potential. It moves to the red and becomes a clear peak with less basic dioxolenes such as ClDiox (Table VIII). These observations lead to a $Ru(d\pi) \rightarrow R'Diox$ MLCT assignment. There are two possible transitions that are expected to be relatively strong, namely $Ru(b_{2g},b_{3g}) \rightarrow R'Diox(b_{1u})$. Since there appear no other reasonable candidates for these transitions in the visible region, they may both fall under the band (O1,I,II) envelope.

At higher energies two weaker absorptions are observed, at 520 and 450 nm (bands (O1,III,IV)). These transitions have no clear correlation with pyridine substituent, but the peak near 450 nm shifts to the blue with less electron-donating dioxolenes. Two dioxolene $n \rightarrow \pi^*$ transitions, $a_g \rightarrow b_{1u}$ and $b_{3u} \rightarrow 2b_{2g}^*$, are allowed in O1. These are analogous to band (S,II) and are assigned to bands (O1,III,IV). Band (O1,V) at 380 nm can be assigned as the internal semiquinone $\pi \rightarrow \pi^*$ transition[55] since MLCT transitions involving the pyridine will be in the UV region and no low-energy LMCT from pyridine is expected.

O2 Species. Owing to general species instability, no detailed spectroscopic analyses were undertaken; upon oxidation of O1, isosbestic points were usually poor or not present. However oxidation of O1 $Ru(3\text{-}ClPy)_2(DTBDiox)_2$ and $Ru(4\text{-}AcPy)_2(DTBDiox)_2$ gave reasonable isosbestic points. The O2 species produced had broad strong bands around 650 nm in DCE.

Table IX summarizes the assignments of transitions observed in the R1, S, and O1 species.

(57) Motten, A. G.; Hanck, K. W.; DeArmond, M. K. *Chem. Phys. Lett.* **1981**, *79*, 541.
(58) Morris, D. E.; Hanck, K. W.; DeArmond, M. K. *J. Am. Chem. Soc.* **1983**, *105*, 3032.
(59) Morris, D. E.; Hanck, K. W.; DeArmond, M. K. *Inorg. Chem.* **1985**, *24*, 977.

Chart III

R2	$[Ru^{II}(RPy)_2(cat)_2]^{2-}$
R1	$[Ru^{III}(RPy)_2(cat)_2]^{-}$
S	$Ru^{III}(RPy)_2(cat)(sq) \leftrightarrow Ru^{II}(RPy)_2(sq)_2$
O1	$[Ru^{III}(RPy)_2(sq)_2]^{+}$

Concluding Remarks

In summary, the *t*-$Ru(RPy)_2(R'Diox)_2$ redox series are best represented as shown in Chart III.

These conclusions differ slightly from the conclusions reached for the corresponding *c*-(bpy) complexes shown in Chart II. Yet, on the basis of similarities in the FTIR and PES spectra and Ru–O and dioxolene bond lengths in the S complexes, $Ru(bpy)(Diox)_2$ and $Ru(4\text{-}BuPy)_2(DTBDiox)_2$, the net electron transfer from the two dioxolenes to the metal (and therefore the degree of metal–ligand orbital mixing) is probably approximately equal in the cis and trans S species.

The real differences between the two series are due to symmetry affecting the distribution of metal and ligand electron density between orbitals. This results in electronic spectroscopic differences which have caused us to reach different conclusions regarding the "best representation" of the electronic structures of the two series.

In the trans species only one of the Ru "t_{2g}" orbitals can mix with the dioxolene π $3b_1$ orbital, whereas in the cis complexes all three t_{2g} orbitals are allowed by symmetry and overlap to mix with the dioxolene $3b_1$ set. Thus in the trans species two metal valence orbitals are nonbonding with respect to the dioxolene, and the b_{1u} level is pure ligand in nature (barring some mixing with metal $p\pi$).

Supposing that, in the S complexes, the valence metal and dioxolene ligand b_{2g} orbitals in the trans species mix to give two orbitals (b_{2g} and $2b_{2g}$*) each of which has approximately 50% metal and 50% ligand character, the "oxidation state" of the metal approximates to Ru^{III} on the basis of the weighted populations of the valence orbitals. The lowest energy electronic transition ($b_{1u} \rightarrow 2b_{2g}$*) then has LMCT character.

In the cis complexes all three metal levels mix with dioxolene π levels. The amounts of mixing will differ for the three orbitals, but if we assume the same net transfer of ligand electron density to the metal as in the trans series above, but now distributed over three d orbitals, we obtain approximate average populations of 70% d + 30% diox for the three "d" orbitals, and 55% diox + 45% d for the ligand π* orbitals. This again gives an "oxidation state" of approximately Ru^{III} (5.1 valence electrons localized on the metal). However, in this case, the lowest energy electronic transition has MLCT (Ru → diox) character, as observed.

Our conclusions relating to the cis complexes were largely influenced by the electronic spectroscopic data for which a Ru^{II} description was most useful (particularly in view of the resonance Raman data showing a Ru → bpy CT transition), although we recognized that the real situation was not clearcut and that a MO picture was needed. Clearly, for the trans species the Ru^{II} description is less useful, since transitions of LMCT character are seen. In the O1 species, the overall degree of metal–ligand mixing may also be similar in the cis and trans species, but there is less evidence available to support this supposition. If this is so, then similar arguments apply.

It is also noteworthy that both the S and O1 species are apparently best described as Ru^{III} species without the normal $4d^5$ configuration, S being diamagnetic and O1 having a hole in a ligand-based orbital.

There are clearly subtle new features arising from the study of redox series involving noninnocent, or redox active, ligands. The variation in ligand substitution in the pyridine series does not have a great influence on the electronic structure of each redox product but is extremely useful in assigning the electronic spectra of these species. Similar work has been completed on phosphine-substituted species, which offer a wider range of variation in the σ and π properties of the coligands[60,61] and on the substitution of the oxygen atoms of the dioxolene ligands by nitrogen.[62]

Acknowledgment. We are indebted to the Natural Sciences and Engineering Research Council (Ottawa) and the Office of Naval Research (Washington, D.C.) for financial support. We also thank Yu Hong Tse for recording some spectroscopic data, Dr. Lawrence Thompson (Memorial University) for magnetic measurements, and the Johnson Matthey Co. for the loan of ruthenium trichloride.

Supplementary Material Available: Listings of analytical data for S (Table SI) and O1 (Table SII) and FTIR data for S (Table SIII) and O1 (Table SIV) (7 pages). Ordering information is given on any current masthead page.

(60) Bhattacharya, S.; Pierpont, C. G. *Inorg. Chem.* **1991**, *30*, 1511.
(61) Auburn, P. R.; Lever, A. B. P. To be submitted for publication.
(62) Masui, H.; Lever, A. B. P.; Auburn, P. R. *Inorg. Chem.* **1991**, *30*, 2402.